PNAS RESEARCH ARTICLE | PLANT BIOLOGY

Dramatic changes in mitochondrial subcellular location and morphology accompany activation of the CO_2 concentrating mechanism

Justin Findinier[a,1], Lydia-Marie Joubert[b], Neda Fakhimi[a], Michael F. Schmid[b], Andrey V. Malkovskiy[a], Wah Chiu[b,c], Adrien Burlacot[a,d], and Arthur R. Grossman[a,d,1]

Affiliations are included on p. 11.

Edited by Ursula Goodenough, Washington University in St. Louis, Chilmark, St. Louis, MO; received April 15, 2024; accepted September 6, 2024

Dynamic changes in intracellular ultrastructure can be critical for the ability of organisms to acclimate to environmental conditions. Microalgae, which are responsible for ~50% of global photosynthesis, compartmentalize their Ribulose 1,5 Bisphosphate Carboxylase/Oxygenase (Rubisco) into a specialized structure known as the pyrenoid when the cells experience limiting CO_2 conditions; this compartmentalization is a component of the CO_2 Concentrating Mechanism (CCM), which facilitates photosynthetic CO_2 fixation as environmental levels of inorganic carbon (Ci) decline. Changes in the spatial distribution of mitochondria in green algae have also been observed under CO_2 limitation, although a role for this reorganization in CCM function remains unclear. We used the green microalga *Chlamydomonas reinhardtii* to monitor changes in mitochondrial position and ultrastructure as cells transition between high CO_2 and Low/Very Low CO_2 (LC/VLC). Upon transferring cells to VLC, the mitochondria move from a central to a peripheral cell location and orient in parallel tubular arrays that extend along the cell's apico-basal axis. We show that these ultrastructural changes correlate with CCM induction and are regulated by the CCM master regulator CIA5. The apico-basal orientation of the mitochondrial membranes, but not the movement of the mitochondrion to the cell periphery, is dependent on microtubules and the MIRO1 protein, with the latter involved in membrane–microtubule interactions. Furthermore, blocking mitochondrial respiration in VLC-acclimated cells reduces the affinity of the cells for Ci. Overall, our results suggest that mitochondrial repositioning functions in integrating cellular architecture and energetics with CCM activities and invite further exploration of how intracellular architecture can impact fitness under dynamic environmental conditions.

CO_2 concentrating mechanism | microalgae | mitochondria | Chlamydomonas | fluorescence microscopy

Significance

Mitochondria often form a dynamic membrane network that can change their intracellular location to sustain adenosine triphosphate (ATP) consumption for specific functions such as synaptic vesicle mobilization in neurons or photosynthesis in plant and algal cells. In this study, we investigated changes in mitochondrial ultrastructure and its subcellular location in the green microalga *Chlamydomonas reinhardtii* and demonstrated the role of microtubules to achieve mitochondrial reorganization when the cells experience very low CO_2 availability. We also gained further insights into the functional importance of mitochondrial respiration and carbonic anhydrases in the context of the CO_2 concentrating mechanism and raise questions about how mitochondrial dynamics can respond to the diverse energetic needs experienced by photosynthetic cells.

Both the intracellular position and ultrastructure of organelles can exhibit dynamic behavior in response to specific stressors or during metabolic shifts (1). Changes in spatial and morphological features of an organelle may be key for completing developmental processes and acclimating to changing environmental conditions. For example, the movement and repositioning of mitochondria in the cell can be required for their proper partitioning between mother and daughter cells in budding yeast (2). They are also critical in animals for optimizing delivery of energy for fueling cell migration (3, 4) and the release of synaptic neurotransmitters (5), and generally require the activity of the cytoskeletal network (6). The movement and repositioning of cellular compartments have also been demonstrated for the ER (7, 8), nuclei (9, 10), and chloroplasts (11).

In microalgae, which mediate ~50% of photosynthesis on Earth (12), major cellular ultrastructural shifts can occur as CO_2 levels change. One change reflects the condensation of most of the CO_2-fixing enzyme Ribulose-1,5-bisphosphate carboxylase (Rubisco) in a membrane-less organelle called the pyrenoid (13). Such a structure is associated with the induction of a CO_2 concentrating mechanism (CCM), which elevates the cell's affinity for inorganic carbon (Ci, which includes CO_2, HCO_3^-, CO_3^{-2}) by actively concentrating CO_2 in the pyrenoid matrix (14).

Dramatic alterations in ultrastructure and intracellular positioning of mitochondria in response to changing CO_2 levels have also been reported (15–17). In the model green microalga *Chlamydomonas reinhardtii* (Chlamydomonas hereafter), the mitochondrial membranes are located mostly within the "cup" formed by the single chloroplast when the cells are grown under conditions of high CO_2 availability (HC, 2 to 5% CO_2 in air, or in the presence of acetate which drives high respiratory CO_2 production). In contrast,

Author contributions: J.F., A.B., and A.R.G. designed research; J.F., L.-M.J., and N.F. performed research; A.V.M. contributed new reagents/analytic tools; J.F., L.-M.J., M.F.S., A.V.M., W.C., A.B., and A.R.G. analyzed data; and J.F. and A.R.G. wrote the paper.

The authors declare no competing interest.

This article is a PNAS Direct Submission.

[1]To whom correspondence may be addressed. Email: jfindinier@carnegiescience.edu or agrossman@carnegiescience.edu.

This article contains supporting information online at https://www.pnas.org/lookup/suppl/doi:10.1073/pnas.2407548121/-/DCSupplemental.

Published October 15, 2024.

as CO_2 availability declines because of a limited supply or increased consumption, the mitochondrial membranes move to the cell periphery and become wedged between the chloroplast outer envelope and the plasma membrane (15, 17). While the functional consequences of these mitochondrial structural modifications remain elusive, their correlation with CCM induction suggests a role in Ci acquisition.

In Chlamydomonas, the major CCM components include carbonic anhydrases (CAHs), and HCO_3^- and CO_2 transporters. They enable the cells to efficiently transport Ci and increase the CO_2 concentration in the pyrenoid (18) where most of the Rubisco resides. Despite evidence that CCM activation is a continuum tightly regulated by CO_2 availability (19), distinct modes of Ci transport are generally considered to operate at i) HC, ii) ambient or low CO_2 (LC, 0.04% CO_2), and iii) very low CO_2 (VLC, <0.02% CO_2) (Fig. 1). In HC, the CCM is inactive, and CO_2 passively diffuses across cellular membranes and into chloroplasts where it is fixed by Rubisco. In LC, most CO_2 diffuses into the cell, is converted into HCO_3^- and trapped in the chloroplast stroma through the activity of LCIB (20, 21). At VLC, the cells mainly actively transport HCO_3^- across the plasma membrane using the HLA3 transporter (22) and move it from the cytoplasm to the chloroplast stroma through the inner envelope membrane channel LCIA (21, 23). In LC and VLC, stromal HCO_3^- is transported to the thylakoid lumen by the bestrophin-like transporters, BST1-3 (24), and is then converted back to CO_2 by CAH3 in the thylakoid tubules that penetrate the pyrenoid (25). The CO_2 then diffuses into the pyrenoid matrix where it is fixed by Rubisco. Also, at VLC the CCM protein LCIB encases the pyrenoid, potentially capturing CO_2 that leaks from the pyrenoid (converting it back to HCO_3^-) (26). Acclimation of Chlamydomonas to LC and VLC depends on CIA5, considered the CCM master regulator (27, 28), and CAS1, a pyrenoid localized calcium sensor protein (29). Mutations that eliminate either of these proteins block the induction of most genes associated with LC and VLC responses (29–32).

In vascular plants, metabolic interactions between mitochondria and chloroplasts play a central role in maintaining the proper functioning of chloroplasts under various conditions (33, 34). In Chlamydomonas, there is evidence that the mitochondrion assumes a new intracellular position and supports CCM function when the cells experience low levels of Ci (15, 17, 35). RNA interference (RNAi) studies showed that CCM activity is impacted by low levels/absence of the mitochondria-localized CAH4/5 proteins and CCP1/2 transporters (35, 36). The authors proposed

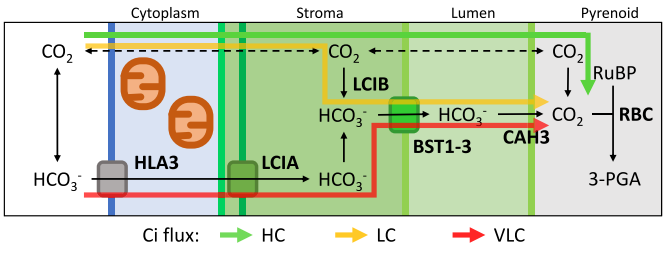

Fig. 1. Modes of CO_2 delivery to Rubisco. At HC, CO_2 passively diffuses to Rubisco (green arrow). At LC, Ci is trapped in the stroma as HCO_3^-, which is facilitated by LCIB activity (yellow arrow). At VLC, HCO_3^- is directly taken up from the medium by the plasma membrane transporter HLA3 and then channeled from the cytoplasm to the stroma by LCIA (red arrow). Stromal HCO_3^- is channeled into the thylakoid lumen through BST1-3 and delivered as CO_2 to the pyrenoid through CAH3 activity. Solid lines: diffusion/transport through membrane protein; dashed lines: diffusion through lipid membrane. Acronyms: CO_2: Carbon dioxide; HCO_3^-: bicarbonate; HLA3: High Light-Activated 3; LCIA: Low CO_2 Induced A; LCIB: Low CO_2 Induced B; BST1-3: Bestrophin 1-3; CAH3: Carbonic Anhydrase 3.

that the mitochondrial CAHs and potential HCO_3^- transporters encoded by CCP1/2 could recapture CO_2 generated by mitochondrial respiration, photorespiration, and/or leakage from the chloroplast by converting it to HCO_3^-, allowing it to be shuttled back into the chloroplast. Mitochondrial respiration has also been proposed to help energize plasma membrane Ci uptake, likely by using reductant generated by chloroplast-to-mitochondria electron flow (37, 38). While mitochondrial relocation has been proposed to play a role in CCM function, it remains unclear to which CCM mode of action it is linked, the molecular mechanisms associated with this dramatic rearrangement, and the specific functions it provides for concentrating Ci.

In this study, we used a mitochondria-targeted fluorophore to monitor mitochondrial relocation as Chlamydomonas cells transition between HC, LC, and VLC conditions. Within 90 min of a transition from HC to VLC, the mitochondria relocate to the cell's cortex with alignment of tubular mitochondrial membranes along the apico-basal axis. This alignment is strongly disrupted when microtubule formation is inhibited and by disruption of a gene encoding a homolog of a microtubule/mitochondrion interacting protein (MIRO1). This dynamic relocation is shown to be under the control of the CCM regulator CIA5 and correlates with relocation of LCIB from a diffuse stromal distribution to being concentrated around the pyrenoid, the induction of CCM genes, including *HLA3* and *CAH4*, and an increase in the cell's affinity for Ci. Furthermore, we show that this change in Ci affinity is inhibited when VLC-maintained cells are exposed to respiratory inhibitors or have a genetic background in which the *CAH4* and *CAH5* genes were disrupted, but not when the apico-basal orientation of the tubular mitochondrial membranes was affected (e.g., in presence of inhibitors of microtubule formation or absence of MIRO1). Overall, our results highlight the kinetic and morphological features of mitochondrial relocation as cells transition to VLC conditions and suggest that the VLC mode of CCM function uses energy generated by mitochondria and depends upon the interconversion of CO_2 and HCO_3^- within the mitochondria.

Results

Dynamics of the Mitochondrial Network Depends on CO_2 Availability. To investigate dynamic changes of the mitochondrial network, we generated a Chlamydomonas strain expressing the GFP variant fluorophore Clover targeted to the mitochondrial matrix (39). The spatial distribution of the network of mitochondrial tubules was then visualized by confocal microscopy (Fig. 2). When cells were grown photoautotrophically (TP medium) in moderate light, sparging cultures with HC or LC resulted in mitochondria mostly positioned within the cup formed by the chloroplast (Fig. 2*A*). Sparging cells with VLC caused the mitochondria to relocate to the cell periphery, between the chloroplast outer envelope and plasma membranes, where they appear as isolated dots and small tubules (Fig. 2*A*). To confirm the physiological state of the cells under the different conditions, we monitored, in a separately generated strain, the position of a fusion protein of the fluorophore mCherry with LCIB, a known marker that reports acclimation of cells to HC/LC and VLC (26). LCIB is diffuse throughout the chloroplast stroma in HC/LC, and only localizes to the perimeter of the pyrenoid in VLC, the same condition that results in mitochondrial localization to the cell periphery (Fig. 2*B*). These results show that mitochondrial relocation occurs in VLC (not HC or LC) acclimated state. We also monitored mitochondrial positioning in the presence of acetate (TAP medium, Fig. 2*C*), which is metabolized and drives a higher

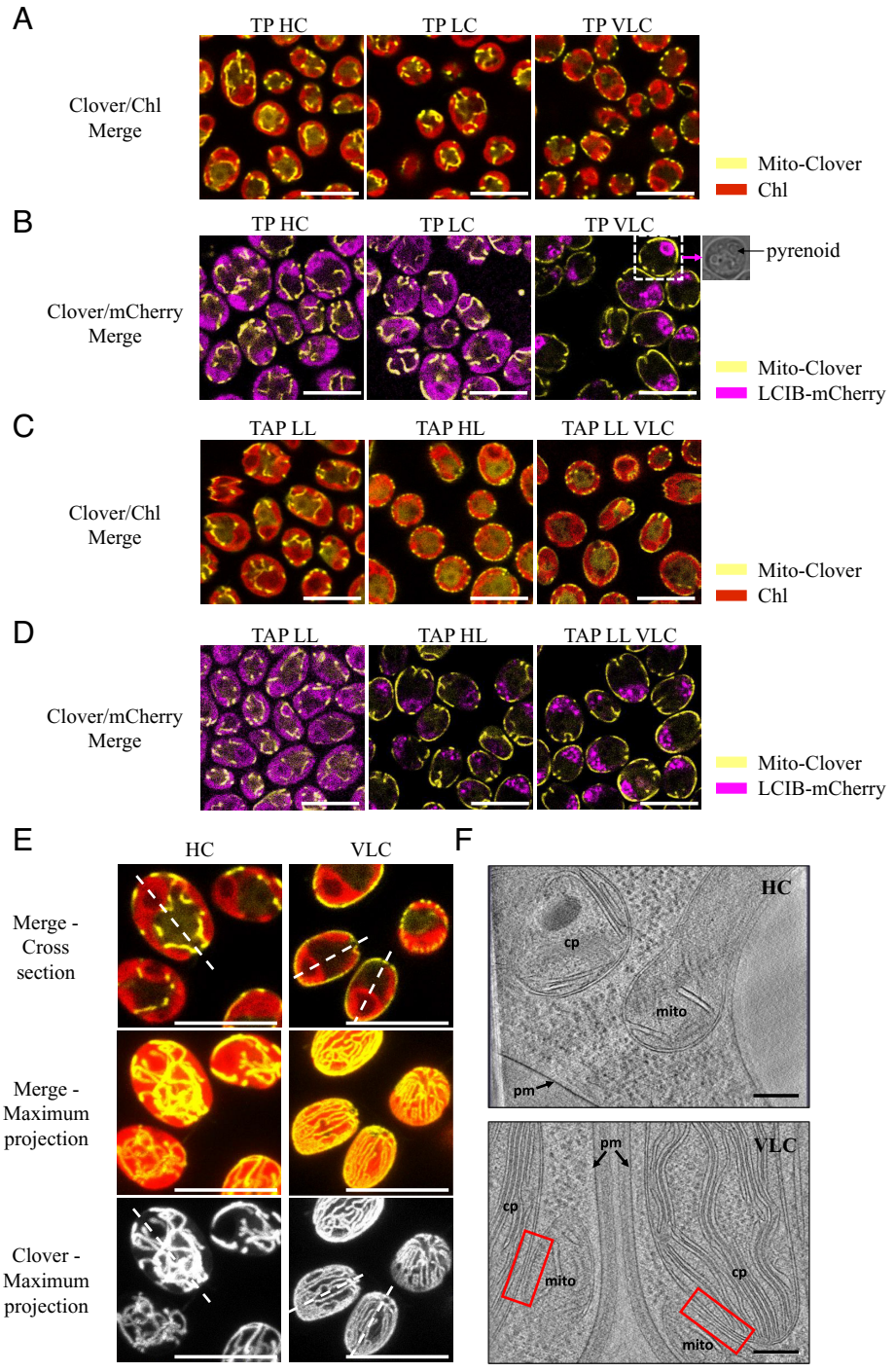

Fig. 2. Physiological conditions and mitochondrial ultrastructure. (*A*) Photoautotrophically grown cells were sparged with HC (~2% in air), LC (0.04%), or VLC (<0.02%) in Tris-Phosphate (TP) buffered medium. Chlorophyll autofluorescence (red) marks the chloroplast while the Clover signal (yellow) marks the positions of the mitochondrial membranes. A weak Clover signal can be observed in the cytosol, which might be a consequence of mistargeting of the protein fusion. (Scale bar: 10 μm.) (*B*) Localization of a LCIB-mCherry fusion (magenta) monitored together with the mitochondria (yellow) in cells sparged with HC, LC, or VLC. The pyrenoid is shown in brightfield for a single cell. (Scale bar: 10 μm.) (*C*) Mitochondria localization was monitored in cells grown without aeration (shaken in flask, 120 rpm), in acetate-supplemented liquid medium (TAP) under LL (30 μmol photons m^{-2} s^{-1}) or HL (500 μmol photons m^{-2} s^{-1}), as indicated, or sparged with VLC in LL. (Scale bar: 10 μm.) (*D*) Localization of a LCIB-mCherry fusion (magenta) monitored together with the position of the mitochondrial membranes (yellow) in cells grown mixotrophically as described in (*C*). Fluorescence from the Chl channel was filtered out. (Scale bar: 10 μm.) (*E*) Mitochondrial membrane locations in cells and their arrangement. Cells were layered on a poly-lysine-coated slide, topped with TP solid medium (1.5% low melting point agarose) and acclimated to HC or VLC conditions for 6 h. Dotted lines highlight the cells' apico-basal axis as observed in cross-sections. (Scale bar: 10 μm.) Fluorescence microscopy images are representative of two experiments. (*F*) Cryo-EM tomogram of HC- or VLC-grown cells showing typical positions of mitochondrial membranes and distances between these membranes (mito) and the chloroplast (cp) or plasma membrane (pm). Red rectangles designate areas of very close proximity of the chloroplast envelope to the mitochondrial outer membrane. (Scale bar: 200 nm.)

respiration rate and an elevated level of intracellular CO_2 (40). The peripheral localization of the mitochondria was readily observed in TAP-grown cells when they were exposed to HL (conditions that drive CO_2 consumption) or sparged with VLC, but not in cells exposed to low light (LL) (Fig. 2*C*). Furthermore, under conditions in which the mitochondria were peripherally located, most of the

LCIB moved to the perimeter of the pyrenoid (Fig. 2*D*). These results further confirmed the specificity of the movement of the mitochondria to the cell periphery under VLC conditions.

When mitochondria are imaged as three-dimensional reconstructions of whole cells (Fig. 2*E*, maximal projections), the tubular mitochondrial membranes appear as a network throughout the cell. Under HC conditions, this network resembles a web of highly reticulated, interconnecting membranes with no dominant orientation (Fig. 2*E*, HC). In contrast, under VLC conditions, the tubular membranes appear elongated over the surface of the chloroplast, oriented parallel to each other and often span the entire length of the cell, connecting at the poles (Fig. 2*E*, VLC, maximal projections). Quantification of the Clover fluorescence signal relative to the chloroplast position revealed a unimodal distribution of mitochondrial membranes at the cell periphery following VLC exposure, whereas in the HC-grown cells, most of the mitochondrial signal was within the inner cup of the chloroplast (*SI Appendix*, Fig. S1). We also used cryoelectron tomography to determine the spatial relationships among mitochondrial membranes, the plasma membrane, and the chloroplast envelope under HC and VLC conditions (Fig. 2*F*). In cells maintained under VLC conditions (Fig. 2*F*, VLC), the mitochondrial membranes were often in close proximity to both the plastid outer envelope and the plasma membrane (Fig. 2*F*, VLC, red rectangle highlights close association between chloroplast and mitochondria). The distance between the outer chloroplast envelope membrane and mitochondrial outer membrane under VLC conditions is here less than 30 nm, extending over the envelope membrane surface of the plastid to lengths of several hundred nm (*SI Appendix*, Fig. S2 and Movies S5–S8). This association at the periphery was not frequently observed in HC samples (*SI Appendix*, Fig. S2 and Movies S1–S4), but we cannot conclude that it does not exist on the inner side (within the cup) of the chloroplast surface.

The kinetics of mitochondrial relocation were analyzed after shifting cells from HC to VLC (*SI Appendix*, Fig. S3 *A* and *B*, *Bottom*). Mitochondrial relocation initiated ~60 min after the shift and was mostly complete by 90 min (*SI Appendix*, Fig. S3*A*). Upon a transition from VLC back to HC, the relocation of mitochondrial membranes to within the chloroplast cup appeared to take more than 120 min and was mostly complete after 180 min (*SI Appendix*, Fig. S3*B*).

We conclude from these experiments that the Chlamydomonas mitochondrial network displays a massive rearrangement in response to VLC conditions, forming parallel, aligned tubules that extend in an apico-basal orientation at the cell periphery; this change in morphology takes about 90 min to complete and is readily reversible. Furthermore, mitochondrial relocation to the periphery appears to be the consequence of diminished intracellular CO_2 levels, which is achieved by either decreasing the supply of Ci (TP, HC/LC to VLC) or by increasing internal CO_2 consumption by photosynthesis (TAP, LL to HL), as suggested previously (17).

Alignment of Mitochondrial Membranes Requires Microtubules. Mitochondrial motility and architecture in various organisms depend upon cytoskeleton components such as actin filaments, microtubules, and intermediate filaments (41), but photosynthetic organisms only harbor microtubules and actin. The Chlamydomonas genome contains genes encoding actin, *NAP1* and *IDA5*, with the latter sensitive to the compound Latrunculin B (LatB) (42). Therefore, we examined the involvement of the actin cytoskeleton in mitochondrial relocation in the *nap1-1* mutant (42). While the absence of NAP1 in the mutant had no effect on mitochondria relocation, treatment of *nap1-1* cells with LatB led to delayed relocation (Fig. 3). Whereas mitochondrial relocation and membrane reorganization were nearly complete in untreated *nap1-1* mutant cells after 90 min (Fig. 3*A*, DMSO 0.1%), a delay in the relocation was apparent in LatB treated *nap1-1* cells; even after 180 min, the cells still displayed a strong mitochondrial signal within the cup of the chloroplast (Fig. 3*A*). This experiment demonstrates that actin filaments are important for the timing of the mitochondrial relocation but are not required for the ultrastructural change of the mitochondria.

The potential role of microtubules in the relocation process was assessed using the microtubule inhibitor Amiprophos Methyl (APM). Treatment with APM did not prevent the HL-triggered relocation of the mitochondrial membrane network to the cell periphery (Fig. 3*B*) but did disrupt the establishment of their apico-basal orientation; the mitochondrial tubules at the cell cortex appeared as an interconnected mesh of short tubules (Fig. 3*B*). Because the arrangement of mitochondrial tubules at the cortex extends from the apex to the base of the cell in a configuration similar to that of the cortical microtubules (43), we investigated colocalization of microtubules and mitochondria at the cortex using immunofluorescence. Mitochondria and microtubules were stained using specific antibodies directed against the mitochondrial CAH4 protein and α-tubulin, respectively (*SI Appendix*, Fig. S4). Cortical microtubules spanned the entire cell length along the apico-basal axis (*SI Appendix*, Fig. S4, TUB) and aligned with mitochondrial membranes when the cells were grown under VLC conditions; this alignment did not occur in HC (*SI Appendix*, Fig. S4, HC Merge).

To further analyze the cytoskeleton requirement for relocation and reorientation of mitochondrial membranes, we investigated the effect of simultaneously eliminating actin and microtubules from the cells by simultaneously treating the *nap1-1* mutant with LatB and APM (*SI Appendix*, Fig. S5). When both drugs are present, the effect is surprisingly severe relative to the loss of the individual cytoskeletal components (actin or microtubules). Mitochondria relocation is strongly inhibited during the first 90 min of exposure to HL (*SI Appendix*, Fig. S5, 90 min). After 180 min, a fraction of mitochondria was at the cell periphery (*SI Appendix*, Fig. S5, 180 min), but they appeared fragmented relative to control conditions, which might reflect whole cell defects that prevent attaining the physiological changes associated with VLC conditions.

In animal cells, mitochondrial interaction with microtubules is mediated by isoforms of MIRO, a conserved GTPase (44). The Chlamydomonas genome contains a single gene encoding a MIRO1 homolog (Cre08.g375200) (*SI Appendix*, Fig. S6). To confirm the localization of MIRO1, we generated a strain expressing this GTPase fused with mCherry at its N terminus. When expressed in VLC-grown cells, the mCherry-MIRO1 fusion aligned with the Clover signal, but also displayed increased intensity near the cell apex in the vicinity of the basal bodies, where cortical microtubules are organized (*SI Appendix*, Fig. S7*A*). Mutants disrupted for *MIRO1* were generated by a CRISPR-guided insertion of a paromomycin resistance cassette in the background strain expressing the mitochondria-targeted Clover fluorophore (*SI Appendix*, Fig. S7*B*). Mutants originating from different insertion events in the *MIRO1* gene had no defect on the relocation of mitochondria to the cell periphery but displayed significant structural aberrations in the mitochondrial membrane pattern under all growth conditions; there were large areas of aggregated/patchy mitochondria and generally lower numbers of mitochondrial membrane tubules that spanned the surface of the chloroplast under VLC conditions (Fig. 3*C* and *SI Appendix*, Fig. S7*C*). Additionally, the microtubule arrangement was not affected in the *miro1* mutants (*SI Appendix*, Fig. S8). These results indicate

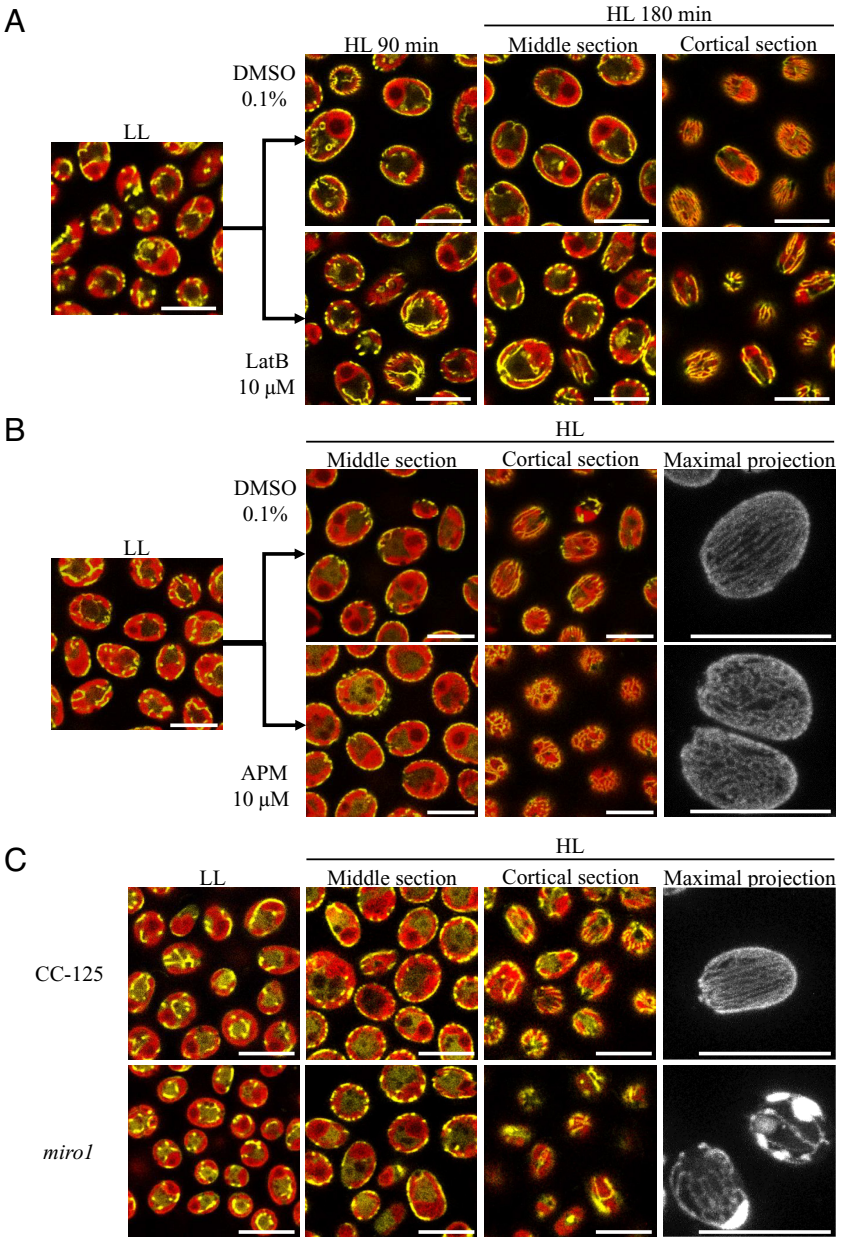

Fig. 3. Involvement of cytoskeleton components on relocation of mitochondrial tubules. (*A*) Effect of Latrunculin B (LatB) on the *nap1-1* mutant. Mitochondrial relocation induced by HL was examined in the *nap1-1* background, in the absence (only DMSO 0.1%) and presence (LatB 10 μM in DMSO 0.1%) of the actin inhibitor LatB. (Scale bar: 10 μm.) (*B*) Effect of APM on mitochondrial location and membrane tubule organization. Mitochondrial relocation was examined in WT cells in the absence (only DMSO 0.1%) and presence of APM (APM 10 μM in DMSO 0.1%); cortical sections showing mitochondrial membrane organization near the plasma membrane and the maximal projections (cells immobilized on 1.5% TP agar) showing the whole cell mitochondrial signal. (Scale bar: 10 μm.) (*C*) Effect of absence of MIRO1 upon HL-induced relocation and the organization of mitochondrial membranes. Mixotrophically grown WT (CC-125) and mutant (*miro1*) cells were exposed to HL to induce mitochondria relocation. Cortical sections and maximal projections show the organization of the mitochondrial network. (Scale bar: 10 μm.) Fluorescence microscopy images are representative of two experiments.

that microtubules and MIRO are required for attaining the parallel organization of mitochondrial membranes at the cell's cortex under VLC conditions.

Mitochondrial Relocation Correlates with CCM Induction and Is Controlled by CIA5. Metabolic processes including photosynthetic electron transport, but also translation and transcription, could potentially be required for reorganization of mitochondrial membranes. To investigate the impact of photosynthesis on this reorganization, we used photosynthetic mutants and specific inhibitors during HL induction of mitochondrial relocation. Upon transfer of mixotrophically grown cells from VLL to HL, a mutant impaired in the primary reaction of photosynthesis (*F64* defective for the CP43 protein, does not accumulate PSII) (45) failed to induce mitochondrial relocation (Fig. 4*A*, *F64*) while control cells exhibited the expected pattern (Fig. 4*A*, CC-124). Similarly, a strain defective for regeneration of the Rubisco substrate ribulose biphosphate by phosphoribulokinase (PRK) (46) was also unable to induce mitochondrial relocation (Fig. 4*A*, *prk*). The use of the PSII inhibitor DCMU or the PRK inhibitor Glycolaldehyde (GA) also inhibited relocation of mitochondrial tubules to the cell periphery (*SI Appendix*, Fig. S9*A*). However, in the *F64* and *prk* mutant strains, the relocation of mitochondria was achieved when cultures where sparged with CO_2-free air (Fig. 4*B*). In contrast, inhibition of mitochondrial respiration with Myxothiazol (MX, respiratory complex III inhibitor) did not block

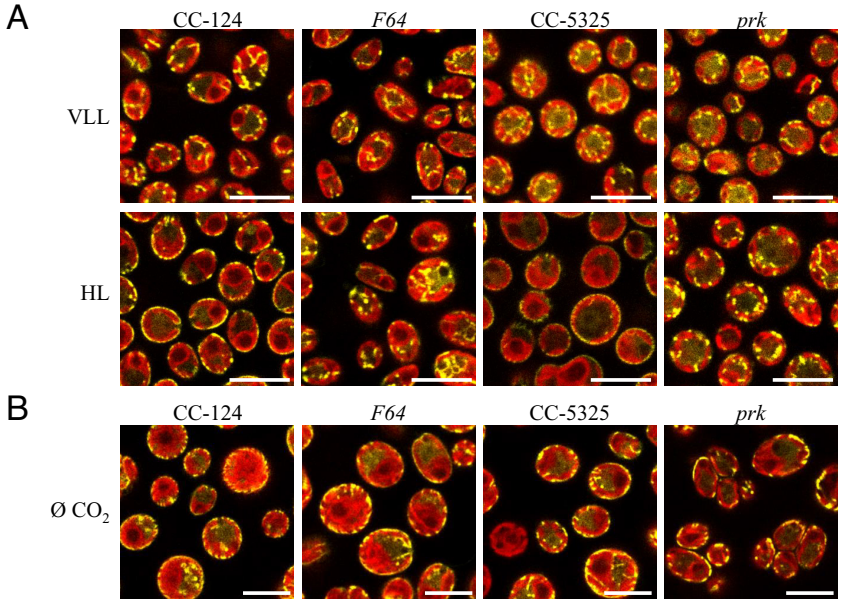

Fig. 4. Effect of mutations that block photosynthesis on mitochondrial relocation/reorganization. (*A*) Effect of PSII and PRK mutations: mutant strains (*F64* and *prk*) and their corresponding parental strains (CC-124 and CC-5325) were mixotrophically grown in very low light (VLL, <5 µmol photons m^{-2} s^{-1}) before being assayed for mitochondrial membrane rearrangement in HL. (*B*) Effect of CO_2 depletion on the position of mitochondria in the *F64* and *prk* mutants: mixotrophically grown cells were sparged with CO_2-depleted air for 6 h and then assayed for their capacity for mitochondrial relocation under VLC conditions. (Scale bar: 10 µm.) Fluorescence microscopy images are representative of two experiments.

the relocation, although it did appear to result in fragmentation of the mitochondrial membrane network (*SI Appendix*, Fig. S9*B*). We conclude that the cellular distribution of mitochondrial tubules depends primarily on the level of CO_2 available to the cells, which is determined by i) the rates of intracellular CO_2 generation and consumption (which depends on respiratory and photosynthetic rates) and ii) the Ci levels present in the environment.

To assess the requirement for de novo gene expression and protein synthesis in driving mitochondrial rearrangements, we examined mitochondrial relocation in the presence of the eukaryotic transcription inhibitor actinomycin D (Act D), the eukaryotic translation inhibitor cycloheximide (CHX), and the chloroplast translation inhibitor chloramphenicol (CAP). Inhibitors of eukaryotic transcription and translation both prevented relocation of the mitochondrial membranes to the cell periphery (Fig. 5*A*) whereas the relocation was unaffected by the prokaryotic translation inhibitor CAP (*SI Appendix*, Fig. S10). A potential effect of the transcription/translation inhibitors on cortical microtubules was tested and showed no difference between control and treated conditions (*SI Appendix*, Fig. S11).

Because of the dependence of mitochondrial positioning on CO_2 levels and de novo transcription/translation, we probed expression of CCM-related genes under the various CO_2 conditions used to determine whether there is a correlation between CCM induction and mitochondrial relocation. We grew the cultures under photoautotrophic conditions and transcript levels of known CCM genes were quantified by RT-qPCR following exposure of the cells to HC, LC, and VLC (same conditions as in Fig. 2*A*). While transcript levels from the gene encoding LCIA increased steadily from HC to LC and VLC, transcripts levels of *HLA3* and the CCM associated mitochondrial genes, *CAH4* and *CCP1*, were only strongly induced when the cells were grown in VLC (Fig. 5*B*). The induction of mitochondria-localized proteins associated with the CCM paralleled mitochondrial relocalization to the cell periphery (Fig. 2*A*).

The correlation of mitochondrial relocation with the induction of CCM genes led us to test whether the former is governed by CIA5, the regulator that controls CO_2-dependent expression of CCM genes (27, 28). We introduced the construct expressing the gene encoding a mitochondria-targeted Clover into the *cia5* mutant (32). VLC exposure of the *cia5* strain did not result in peripheral mitochondrial localization (Fig. 5*C*, *cia5*) whereas this rearrangement was observed in the parental control strain (Fig. 5*C*, CC-125). Upon prolonged sparging with air completely depleted of CO_2 (9 h), the *cia5* mutant was still unable to perform mitochondria relocation and instead displayed a reduced mitochondrial signal that was often located near the apex of the cell; this behavior might indicate a strong decline in the health of the cells (*SI Appendix*, Fig. S12*C*). Ectopic expression of a WT copy of the *CIA5* gene in the *cia5* mutant (*SI Appendix*, Fig. S12) restored the strain's ability for relocation (Fig. 5*C*, *cia5*-C1), demonstrating that CIA5 is integral to the relocation process. We also found that a mutant in the Ca^{2+} binding CAS1 protein, also linked to CCM gene expression (29), showed normal mitochondrial relocation (*SI Appendix*, Fig. S13). We conclude that changes in the mitochondrial position and architecture upon acclimation of Chlamydomonas to VLC are controlled by the CCM regulator CIA5, but not CAS1, and that they parallel changes in expression of the CCM-related genes.

Mitochondrial Relocation Is Correlated with an Increased Impact of Respiration on CCM Function. To further explore a potential role of changes in mitochondrial position/ultrastructure on CCM activity, we measured Ci-dependent O_2 evolution in WT cells to evaluate the apparent affinity of the cells for Ci under HC, LC, and VLC conditions. Under LC conditions, CCM activation increases the cells' affinity for Ci compared to HC, as shown by the reduced $K_{1/2}$ value for Ci uptake (Fig. 6*A*), the concentration required to reach half maximum O_2 evolution capacity. Growth under VLC conditions further increased the cell's affinity for Ci (Fig. 6*A*).

To examine the potential role of mitochondrial electron transport on CCM activity, the cells were treated with the respiratory inhibitors MX and salicylhydroxamic acid (SHAM, alternative oxidase [AOX] inhibitor), as described in Burlacot et al. (37). While MX/SHAM treated VLC-grown cells showed a marked decrease in their

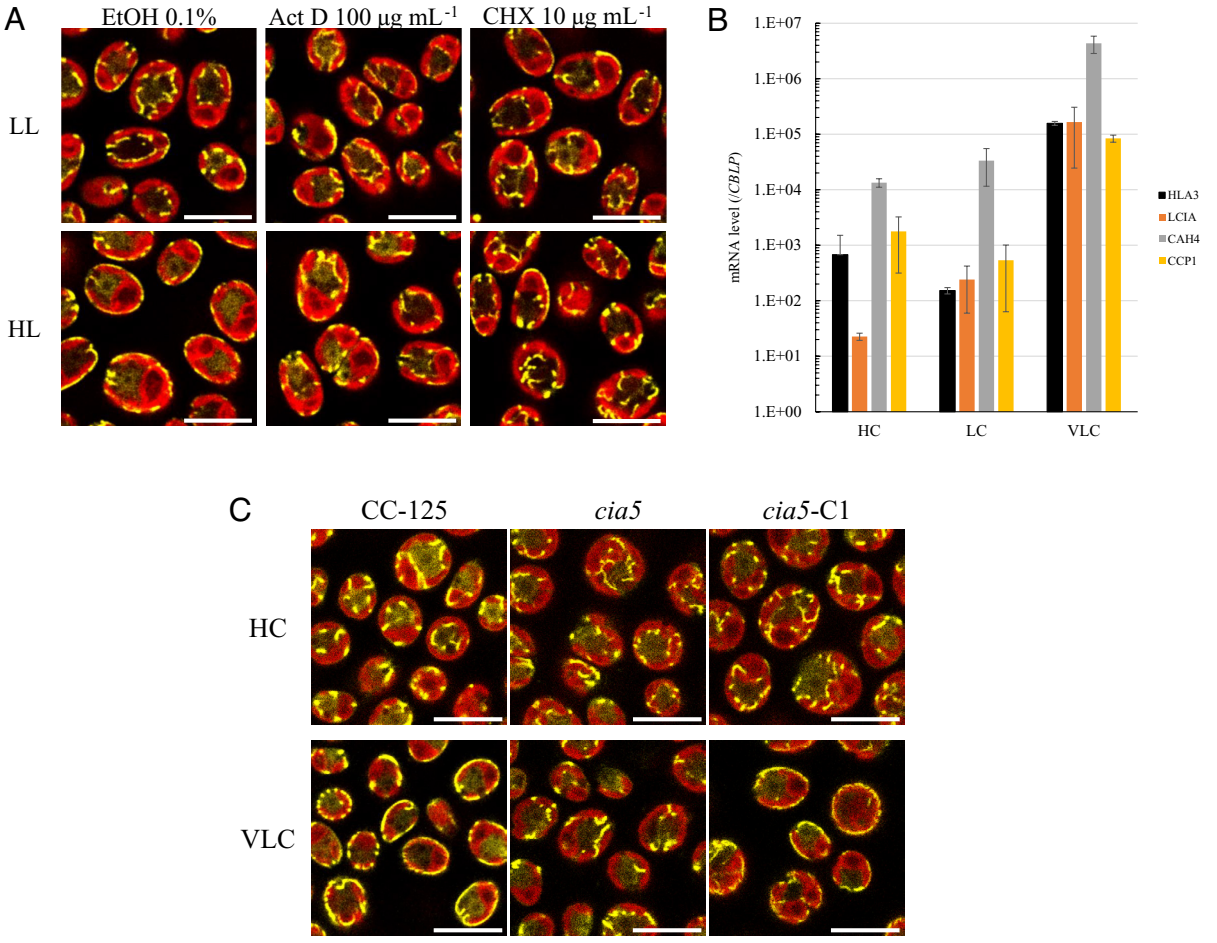

Fig. 5. Relationship of mitochondrial relocation to the CCM. (*A*) Effect of transcription and translation inhibitors. Cells were grown in TAP LL before HL treatment in the presence of ethanol (EtOH 0.1%), the inhibitor of nuclear transcription, actinomycin D (Act D), or the inhibitor of translation on 80S ribosomes, cycloheximide (CHX). Control cells were incubated in LL in the presence of the drugs. (Scale bar: 10 µm.) (*B*) Induction of CCM genes under conditions that cause movement of mitochondria to the cell periphery. The level of induction of genes encoding HLA3, LCIA, CAH4, and CCP1 in cultures sparged with HC (2% CO_2), LC (air), and VLC (CO_2-depleted air; <0.02%); all cultures were exposed to 100 µmol photons m^{-2} s^{-1}. (*C*) Dependence of mitochondrial relocation on CIA5. Wild-type (CC-125), the mutant (*cia5*), and the complemented (*cia5*-C1) cells were grown photoautotrophically in HC and tested for mitochondrial relocation following 4 h of VLC treatment. (Scale bar: 10 µm.) Fluorescence microscopy images are representative of two experiments.

apparent affinity for Ci (increased $K_{1/2}$ value, Fig. 6*B*), LC-grown cells did not show a significant affinity difference upon MX/SHAM treatment (Fig. 6*B*). It is important to notice the difference between our observations and the results from Burlacot et al. (37) at LC, which likely stem from differences in culture conditions. We grow Chlamydomonas cells with air bubbling which allows better equilibration of CO_2 levels while Burlacot et al., used shaken flasks, probably generating a lower effective Ci concentration in the culture medium, especially as the culture density increases. Each inhibitor was also used individually, with no effect for SHAM and a small but significant impact for MX under VLC conditions (Fig. 6*B*). We also tested cells disrupted for the apico-basal organization of the mitochondrial membrane network in both a mutant lacking the MIRO1 protein and WT cells treated with APM. Neither the mutant cells nor the APM-treated WT cells showed a difference in their ability to grow under VLC conditions (*SI Appendix*, Fig. S7) or their affinities for Ci relative to untreated WT cells (*SI Appendix*, Fig. S14 *A* and *B*).

Because it has been proposed to contribute to mitochondrial ATP production (38), we also tested the effect of inhibition of the photorespiratory pathway using the pyridoxal-phosphate analog aminooxyacetate (AOA), which inhibits transaminase reactions, including the reaction that converts glyoxylate to glycine during photorespiration, and results in the excretion of the accumulated intermediate glycolate (47) (*SI Appendix*, Fig. S14*C*). We observed a decrease in the affinity of VLC grown cells for Ci after a 30 min exposure to AOA, but no effect was observed in LC (Fig. 6*C*).

We also tested the impact of the absence of two mitochondrial carbonic anhydrases, CAH4 and CAH5, known to be highly induced upon activation of the CCM and to be involved in CCM function (35). We generated knockout mutants for both *CAH4* and *CAH5* (*SI Appendix*, Fig. S15*A*) and investigated their fitness and Ci affinity under VLC conditions versus LC conditions. We initially confirmed that the *cah4/5* double mutants were not impaired in their capacity to relocate mitochondria to the cell periphery (*SI Appendix*, Fig. S15*C*). When incubated under LC conditions, the *cah4/5* mutants grew normally compared to the parental WT cells, but their growth was impaired under VLC conditions (*SI Appendix*, Fig. S15*B*). Additionally, the mutants exhibited no difference in their affinity for Ci under LC conditions (Fig. 6*D*, LC) but had a lower affinity for Ci when grown in VLC (Fig. 6*D*, VLC). From these experiments we conclude that mitochondrial relocation in VLC is associated with an increase in the cell's affinity for Ci, which occurs through the combined effects of respiratory activity, the activity of the mitochondrial CAH4/5 proteins, and potentially photorespiration.

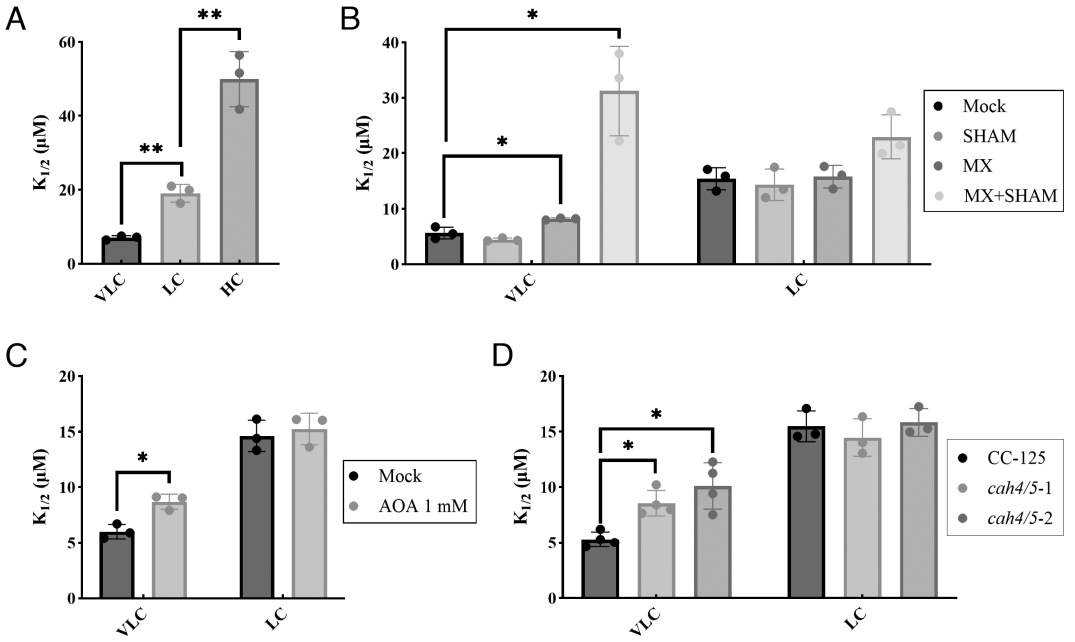

Fig. 6. Analysis of mitochondrial inhibitors and mutants on the affinity of the cells for Ci (pH 7.8). (*A*) Ci affinity in WT cells grown in HC, LC, and VLC conditions (n = 3). (*B*) Effect of the inhibitors SHAM and MX, separately and simultaneously on Ci affinity in cells grown in VLC and LC conditions. Inhibitors were added just prior to the assay (n = 3). (*C*) Effect of the aminotransferase inhibitor AOA (1 mM) on Ci affinity at VLC and LC. Cells were preincubated for 30 min in the presence of AOA (n = 3). (*D*) Ci affinity in the *cah4/5* mutants grown in LC and VLC conditions, compared to the WT parental strain (CC-125) (VLC, n = 4; LC, n = 3). **P* value < 0.05. ***P* value < 0.005.

Discussion

Mitochondrial relocation during acclimation of Chlamydomonas to low CO_2 was first observed by electron microscopy in the work of Geraghty and Spalding (15). Apart from significant vacuolization of the cells, probably a consequence of damaged chloroplast content and degradation of cellular components, the most striking change during acclimation of cells to low levels of Ci was the relocation of mitochondria to the cell periphery where they are wedged between the chloroplast outer envelope and the plasma membrane (15). In this work, we investigated conditions and molecular factors required to induce and accomplish the peripheral positioning and changes in the structural organization of the mitochondrial network as the cells transition from HC to LC/VLC.

Relocation of the mitochondrial membrane network to the cell periphery was observed in photoautotrophic cultures that were experiencing VLC levels or when exposed to HL in acetate-containing medium, suggesting that peripheral mitochondrial localization might be a feature of VLC acclimated cells (below ambient levels of CO_2), which was supported by its correlation with the relocation of LCIB to the perimeter of the pyrenoid (VLC is required for LCIB relocation). Suppression of photosynthetic CO_2 fixation using inhibitors or photosynthetic mutants prevented HL-induced relocation, which occurred when the cultures were sparged with VLC. These results indicate that the signal triggering the rearrangements strongly depends on Ci availability in or around the cells, which is dictated by the balance between internal CO_2 production, stimulated by acetate assimilation and respiration, photosynthetic CO_2 fixation, which is elevated as the light levels increase, and the level of external Ci. Given the importance of Ci conditions and CO_2 production/consumption by the cells, we investigated and confirmed the link between mitochondria relocation and CCM induction. Indeed, conditions that triggered mitochondrial redistribution were strongly associated with transcriptional induction of CCM genes; the relocation was also dependent on CIA5, a protein critical for CCM induction. Together, our findings indicate that the Ci concentration is not only critical for controlling the CCM activity but is also a major factor that impacts the spatial distribution of the mitochondrial network in the cell.

Various hypotheses regarding a role for mitochondrial relocation to the cell periphery during VLC growth are depicted in Fig. 7. A recent study showed that the mitochondrial CAH4 and CAH5 proteins are required for optimal growth at low CO_2 concentrations and contribute to Ci uptake (35). Our investigation of *cah4/5* mutants showed a phenotypic defect even though the mitochondria achieved a peripheral location. Potentially, the CAHs could recycle the CO_2 generated by mitochondrial respiration and photorespiration (e.g., routing Ci back to the chloroplast), but the peripheral mitochondrial position could also allow recapture of CO_2 that might leak from the pyrenoid after HCO_3^- is converted to CO_2 by CAH3. In this case, the mitochondrion would form an additional barrier to CO_2 leakage, augmenting the

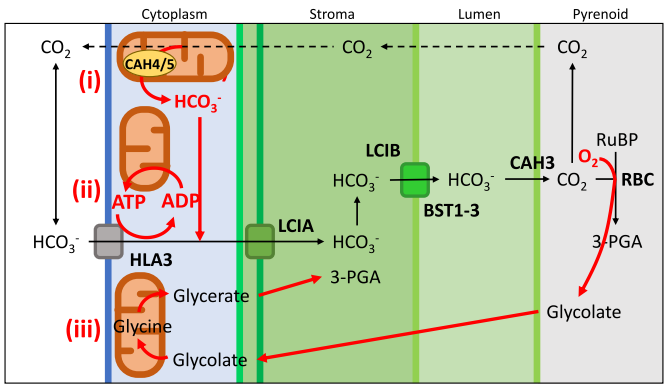

Fig. 7. Possible roles of mitochondrial relocation to the cell cortex. (i) Mitochondrial CAH4/5 could capture CO_2 that leaks from the chloroplast and channel it back into the chloroplast. (ii) Mitochondrial respiration can provide energy in the form of ATP for the active uptake of HCO_3^- at the plasma membrane. (iii) Mitochondria can intercept glycolate and metabolize it through the photorespiratory pathway to limit the loss of Ci.

role associated with the starch sheath and the LCIB protein (putative CAH), both of which are positioned at the pyrenoid periphery under VLC conditions. Mitochondria could also form a physical barrier at the cell's periphery to optimize the recycling of glycolate, an intermediate of photorespiration that is exported by the chloroplast and further metabolized by mitochondria but can be excreted by cells during induction of the CCM and photorespiratory enzymes (47).

The *miro1* mutants displayed alterations in the alignment of the mitochondrial membrane network, although the relocation of the organelle to the cell periphery was normal under VLC conditions. Instead of having regularly spaced, parallel membrane tubules spanning the length of the cells, *miro1* cells had a reduced number of mitochondrial membrane tubules, leaving large areas of the chloroplast surface devoid of mitochondrial membranes. However, CCM induction and function in response to VLC were not impaired in the mutants despite the clear reduction in chloroplast surface coverage by mitochondria. These findings suggest that the principal function of mitochondrial relocation is unlikely to be that of limiting CO_2 or glycolate leakage from the cell.

Mitochondria may also contribute to CCM function by providing ATP to energize HCO_3^- transporters (HLA3) on the plasma membrane (37). Spatially optimizing the site of ATP supply and utilization has been observed in neuronal cells and during development (3, 4, 48). The peripheral mitochondrial localization could physically optimize the use of energy resulting from colocalization of respiratory ATP production and consumption by plasma membrane Ci transporters. We currently favor this hypothesis since inhibition of complex III by MX impacts the cell's affinity for Ci under VLC conditions while SHAM had no apparent effect. Indeed, the complex III pathway promotes translocation of two more protons than the AOX pathway and its inhibition has a more severe impact on ATP production than does the inhibition of AOX. This hypothesis is congruent with the finding that mitochondrial relocation is a VLC response since, under VLC conditions and according to Wang and Spalding (21), the cells mostly rely on HCO_3^- uptake from the environment, which would require plasma membrane and chloroplast envelope HCO_3^- transport activity. Under such conditions, HLA3 activity can be supported by mitochondrial respiration while the LCIA channel would mediate passive HCO_3^- diffusion (23). Additionally, the plasma membrane putative H^+ exporting ATPase ACA4, which is proposed to aid HCO_3^- uptake (49), may also benefit from the mitochondrial ATP supply.

Participation of mitochondria in CCM function has also been observed in other algae. While the structural dynamics of mitochondria in response to Ci limitations have not been broadly studied, rearrangements of mitochondria similar to those observed in Chlamydomonas have been noted in *Scenedesmus obliquus* (16) and suggested for *Chlorella ohadii* (50) and *Volvox africanus* (51). In diatoms, mitochondria are strikingly different from those of Chlamydomonas; they are much less reticulated and more globular, which may impact their potential for major rearrangements. However, there is evidence of physical interactions of mitochondria and chloroplasts that may be modulated by growth conditions, possibly promoting the exchange of metabolites between these organelles (52). Additionally, *Phaeodactylum tricornutum* has been shown to induce expression of the gene encoding mitochondrial phosphoenolpyruvate carboxylase (PEPC) when Ci becomes scarce (53), which possibly participates in anaplerosis by HCO_3^- acquisition in the form of oxaloacetate, while under low CO_2 conditions *Thalassiosira pseudonana* expresses mitochondria-localized CAHs (54). In *Nannochloropsis oceanica* (family Eustigmataceae), recent studies have also suggested the importance of the mitochondrial PEPC and CAH for optimal growth under limiting Ci condition (55, 56). Despite its partial use of an apparent C4-type biochemical CCM, *N. oceanica* also relies on a biophysical CCM in which LC-induced, mitochondrial CAHs could be involved, as indicated by the lower fitness of specific RNAi strains under LC conditions (55). *T. pseudonana* also maintains mitochondria-targeted CAH activity (54). Intriguingly, a peripheral mitochondrial position has also been observed in nonphotosynthetic relatives of Chlamydomonas (57–60), which suggests that the peripheral location captures some function(s) not exclusively associated with supporting photosynthesis.

While VLC-induced relocation is readily observed by fluorescence microscopy, it is reasonable to assume that the subcellular localization of mitochondria can be tailored to locally provide energy/ATP to various cellular processes. In Chlamydomonas, a portion of mitochondrial tubules is consistently observed around the contractile vacuoles and their movement tracks the rhythmic beating of the vacuole (Movies S9–S11), likely providing ATP for vacuolar proton pumping ATPases. The close association between mitochondria and chloroplasts could also optimize the use of mitochondrial-generated energy for the import of proteins through the TIC–TOC complex, which is mainly localized near the plastid lobes (49).

The movement and positioning of mitochondria occur in many organisms in addition to algae and have been shown to be dependent on the actin and microtubule cytoskeleton proteins (41); this phenomenon remains poorly understood in plant cells, and even more so in algae like Chlamydomonas. In our work, neither actin nor microtubule cytoskeleton inhibition prevented mitochondrial relocation to the periphery. However, the striking parallel organization of mitochondrial membrane tubules is dependent on the microtubules, to which the mitochondrion probably attaches. An association between microtubules and mitochondria at the cell's cortex under VLC conditions may be mediated by adaptor proteins that link microtubules to the outer mitochondrial membrane, such as MIRO1, a protein critical for mitochondrial network dynamics in mammals, yeast, and plants (61–63). Inactivation of the *MIRO1* gene dramatically impacted the parallel arrangement of mitochondrial membranes but the mitochondria still relocated to the cell periphery upon exposure to VLC. A more in-depth investigation of mitochondrial movement will be necessary to identify those molecular players involved in repositioning the mitochondrial to the cell periphery.

Despite the striking correlation between mitochondrial organization and its spatial location in the cells upon induction of the CCM, it is not clear how important this structural flexibility is for growth under VLC conditions. Therefore, elucidating the molecular mechanisms associated with mitochondrial movement might not be amenable to a mutant screen for altered growth under VLC conditions. One promising strategy would involve screening for mutants unable to perform VLC-induced mitochondrial relocation based on single-cell imaging. To this end, intelligent image-assisted cell sorting (64) is being used to develop high-throughput screening of insertional mutants. This system has been used for screening Chlamydomonas transformants that are unable to concentrate LCIB around the pyrenoid when the cells are shifted to VLC (64). Our preliminary results have demonstrated the feasibility of enriching for "relocation" mutants based on the movement of mitochondria to the cell periphery under VLC conditions (39). This technology will help elucidate the importance of mitochondrial relocation under VLC conditions and identify genes/proteins required for this redistribution.

Materials and Methods

Strains. CC-125 and the *cia5* mutant (32) were provided by Dimitris Petroutsos (CEA, Grenoble, France). The photosynthetic mutant F64 was a gift from the Institut de Biologie Physico-Chimique (IBPC, Paris, France) (45); it was compared to its parental strain, CC-124. The *prk* mutant was a gift from Pierre Crozet (Sorbonne Université, Paris, France) (46) and the *cas1* mutant was ordered from the CLiP library (LMJ.RY0402.131739) (65). The parental strain for both mutants is CC-5325. The actin mutant *nap1-1* was a gift from Masayuki Onishi (Duke University, Durham, USA) (42). The WT strain WT222+ was used for generating cryo-ET images. Strain CSI_FC1D06 constitutively expresses the mitochondrial localized CAH4 protein (Cre05.g248400) fused to the Venus fluorophore (49). This construct has been useful for viewing mitochondria by immunofluorescence in HC and VLC. All newly generated strains are available at the Chlamydomonas Resource Center (https://www.chlamycollection.org/, *SI Appendix*, Table S1).

Plasmid Construction. The plasmid expressing a mitochondria-targeted Clover fluorophore was constructed from components of the Modular Cloning kit for Chlamydomonas (66). The Clover gene (B3-B5) was fused to the sequence encoding the mitochondrial matrix HSP70C targeting peptide (B2) and the fusion protein was expressed under the control of the pAR promoter (A1-B1, HSP70A/RBCS2 fusion promoter) (67) and the PSAD terminator (B6-C1) (68). This construct was assembled in the pAGM8031 plasmid (69) which harbors the hygromycin resistance cassette unless the target strain was already hygromycin resistant, in which case paromomycin resistance was used for selecting transformants. The *LCIB* gene was cloned into the pLM006 backbone (49) in-frame with the mCherry fluorophore sequence using primers listed in *SI Appendix*, Table S2.

The *MIRO1* gene was cloned into the pSLSpec backbone (pSL18 modified to encode spectinomycin resistance) in an N-terminal fusion (MIROs are tail-anchored proteins) with mCherry that was generated by Gibson assembly (New England Biolabs, Ipswich, MA; see primers in *SI Appendix*, Table S2). The pSLSpec plasmid was linearized with NdeI and three segments of the *MIRO1* gene (5′ 479 bp from start codon, 8,137 bp fragment from PTQ2712 SalI/MluI restriction, 3′ 647 bp to the end of 3′UTR) were inserted into the vector just downstream of the mCherry coding sequence that was amplified from pLM006 (49). pSLSpec-mCherry-MIRO1 was linearized and transformed into the *miro1* mutant.

Culture Conditions. Cells were maintained on TAP agar medium for long-term storage. Appropriate antibiotics were included in the solid medium to avoid the loss of expression of the introduced fluorophore. Batch cultures were grown in liquid TAP medium at low light (LL, 30 μmol photons m^{-2} s^{-1}) or very low light (VLL, <5 μmol photons m^{-2} s^{-1}), and the cells were diluted and allowed to grow overnight to ensure logarithmic growth at the time of the assay.

For determining the distribution of mitochondrial membranes under different light intensities and in the presence of different carbon sources, cultures were inoculated at 1 μg Chl mL^{-1} in either 30 mL of medium in 125 mL Erlenmeyer flasks that were stoppered with aluminum foil, or in 50 mL of medium in 2.5 cm wide, 20 cm long glass tubes with aeration from the bottom provided by a Pasteur pipette. The cells were grown for 24 h under various conditions, as specified in the text. VLC conditions were created by bubbling air twice through 50% sodium hydroxide, which reduced the CO_2 level in the medium to ~150 ppm as determined by measurements with an Amprobe CO_2 meter (Everett, WA). Complete CO_2 depletion in air was achieved by passing air through two 2 L bottles filled with soda lime pellets.

For imaging the mitochondrial membrane distribution, the cells were concentrated and layered on a poly-lysine-coated 8-chamber slide (Ibidi, Martinsried, Germany) and topped with 300 μL of 1.5% low-melting point agarose in TP/MOPS medium at 34 °C. Cells were incubated at 100 μmol photons m^{-2} s^{-1} under HC or VLC atmosphere for 6 h to allow for recovery from mild temperature shock and to stabilize the mitochondrial membrane distribution. For monitoring relocation kinetics, the cells were layered on a slide in TP medium as described. Redistribution of mitochondrial membranes was induced by exposure of HC-maintained cells to ambient conditions (ambient levels of CO_2 at 100 μmol photons m^{-2} s^{-1}). After stabilization of the peripheral mitochondrial distribution (6 h minimum), the light was turned off to allow the mitochondrion to revert back to a more internal (central in the cell) mitochondrial membrane distribution.

When testing drugs and specific mutants, induction of mitochondrial membrane relocation was performed under mixotrophic conditions. Cells were grown in TAP medium at LL (or VLL for photosynthetic mutants) and a 5 mL aliquot was exposed to HL for 3 h. GA (5 mM), DCMU (10 μM), MX (2.5 μM), SHAM (400 μM), CHX (10 μg mL^{-1}), Actinomycin D (10 μg mL^{-1}), AOA (1 mM), and APM (10 μM) were purchased from Sigma-Millipore (Saint-Louis, MO, USA), and Latrunculin B (10 μM) from Abcam (Cambridge, UK). A 1 mL aliquot of cells at 1 to 2 × 10^6 cells mL^{-1} was concentrated 20-fold after pelleting the cells by centrifugation for 1 min at 1,500 × g. The concentrated suspension was deposited on a poly-lysine-coated 18-well slide (Ibidi, Martinsried, Germany).

For cryoelectron tomography, WT222+ cells were grown to mid-log phase in TAP medium, pelleted by centrifugation, washed once with High Salt Medium (HSM), resuspended in a small volume of HSM and diluted in TAP or HSM to an $OD_{750\,nm}$ of 0.1. The cells were then allowed to acclimate to the fresh medium in the dark (TAP) or at 60 μmol photons m^{-2} s^{-1} (HSM) for 24 h.

Confocal Microscopy. A TCS SP8 confocal laser-scanning microscope (Leica) with imaging conditions/settings as follows: cells were imaged using LASX software at a ×63, numerical aperture, and a 1.4 oil objective. Excitation/emission settings were 514 nm (notch filter)/525 to 550 nm HyD1 SMD hybrid detector for Clover, and 514 nm/680 to 720 nm HyD2 SMD hybrid detector for chlorophyll autofluorescence, working in parallel. The EM gain was set at 100%. Clover fluorescence was captured with a lifetime gate filter (0.6 to 10 ns) to reduce background noise from chlorophyll autofluorescence. When capturing LCIB-mCherry fluorescence, the settings were 561 nm (notch filter)/591 to 620 nm HyD2 SMD hybrid detector, with the gain set at 500%. Z-stacks were collected at 0.2 μm intervals to generate maximum projections. Images were analyzed using Fiji software.

Cryoelectron Tomography. After 24 h of culturing Chlamydomonas cells either in VLC (HSM, 60 μmol photons m^{-2} s^{-1}) or HC (TAP, Dark), specimens were vitrified by plunge-freezing 3 μL aliquots of the cell suspension onto glow-discharged Quantifoil Multi A Holey Carbon Au 200 mesh TEM grids (SPI Supplies, USA) using a Leica EM GP2 apparatus (Leica, Austria), in which the humidity was kept at under 95% with 4 to 8 s of single-sided blotting on the reverse side of the grid. Ultrathin lamellae (150 to 200 nm) were prepared using an Aquilos2™ cryogenic Focused Ion Beam Scanning Electron Microscope (cryoFIB-SEM, ThermoScientific, USA), operated using a 2 to 5 kV electron beam, a 30 kV Ion beam with the ion probe current adjusted from 0.3 nA to 30 pA for rough milling to final polishing. Grids were transferred under cryogenic conditions to a 300 kV Krios™ cryogenic Transmission Electron Microscope (cryo-TEM, ThermoScientific, USA) with a Gatan K3 detector and BioQuantum energy filter (Gatan Inc, USA) for cryo-ET data collection, which used a pixel size of 3.4 Å, a −60 to 60 degrees tilt range at 2-degree increments, and Serial EM software for automated data collection (70). Tomograms were generated using IMOD software (71) followed by segmentation and visualization using EMAN2 (72) and USCF Chimera (73).

Transcript Quantification. HC, LC, and VLC grown cells were pelleted for 2 min at 800 × g, the supernatant discarded, and the pellet flash frozen in liquid nitrogen. Total RNA was extracted using the Qiagen RNA easy extraction kit following the manufacturer's instructions. cDNA was synthesized from total RNA using the iScript Reverse Transcription Supermix (Bio-Rad, Hercules, CA, USA) with 1 μg of RNA in a 20 μL reaction volume. cDNAs were diluted to 50 μL and used as template for Real-Time PCR monitored by the SensiFast SYBR No-Rox Kit (Bioline, Cincinnati, OH, USA). RT-PCR was performed in the Roche Light Cycler 480 using primers for *CAH4*, *CCP1*, *LCIA*, *HLA3,* and *CBLP* (*SI Appendix*, Table S3).

Oxygen Evolution Measurements. HC, LC, and VLC-grown cells were pelleted for 3 min at 1,800 × g and resuspended to 20 μg Chl mL^{-1} in 2 mL of fresh medium (TP pH 7.8) that was sparged with CO_2-free air. The cells were then loaded into the sample chamber of an Oxygraph+ oxygen electrode system (Hansatech, Norfolk, England). The chamber was sealed and the cells were exposed to 300 μmol photons m^{-2} s^{-1}. Once the O_2 evolution rate declined to net zero, $NaHCO_3$ was added to the suspension at a final concentration of 10, 50, 250, and 1,250 μM and the O_2 evolution rate measured. The $K_{1/2}$(Ci) was calculated from the fitted curve for each strain. AOA was added at 1 mM to the cell culture 30 min prior to measurements of O_2 evolution. MX and SHAM were added at 2.5 μM and 400 μM, respectively, during the CO_2 depletion period.

Data, Materials, and Software Availability. All study data are included in the article and/or supporting information.

ACKNOWLEDGMENTS. This project was supported by funding from Department Of Energy award DE-SC0019417 (to A.R.G.) and BERFWP 100463 (to W.C.). J.F. was supported by the Biosphere Science and Engineering Division of the Carnegie Institution for Science. Some of this work was performed at the Stanford-SLAC Cryoelectron Tomography Specimen Preparation Center, which is supported by the NIH Common Fund's Transformative High Resolution Cryoelectron Microscopy program (U24GM139166). We would like to thank the Carnegie Advanced Imaging Facility for use of microscopy instruments (Leica TCS SP8 confocal laser-scanning microscope).

Author affiliations: [a]The Carnegie Institution for Science, Biosphere Sciences and Engineering, Stanford, CA 94305; [b]SLAC National Accelerator Laboratory, Division of CryoElectron Microscopy and Bioimaging, Menlo Park, CA 94025; [c]Department of Bioengineering, Stanford University, Stanford, CA 94305; and [d]Biology Department, Stanford University, Stanford, CA 94305

1. P. van Bergeijk, C. C. Hoogenraad, L. C. Kapitein, Right time, right place: Probing the functions of organelle positioning. *Trends Cell Biol.* **26**, 121–134 (2016).
2. T. Klecker, D. Scholz, J. Förtsch, B. Westermann, The yeast cell cortical protein NUM1 integrates mitochondrial dynamics into cellular architecture. *J. Cell Sci.* **126**, 2924–2930 (2013).
3. A. Garde *et al.*, Localized glucose import, glycolytic processing, and mitochondria generate a focused ATP burst to power basement-membrane invasion. *Dev. Cell* **57**, 732–749.e7 (2022).
4. M.-H. Schuler *et al.*, MIRO1-mediated mitochondrial positioning shapes intracellular energy gradients required for cell migration. *Mol. Biol. Cell* **28**, 2159–2169 (2017).
5. P. Verstreken *et al.*, Synaptic mitochondria are critical for mobilization of reserve pool vesicles at Drosophila neuromuscular junctions. *Neuron* **47**, 365–378 (2005).
6. A. S. Moore, E. L. F. Holzbaur, Mitochondrial-cytoskeletal interactions: Dynamic associations that facilitate network function and remodeling. *Curr. Opin. Physiol.* **3**, 94–100 (2018).
7. J. Sun, M. Zhang, X. Qi, C. Doyle, H. Zheng, Armadillo-repeat kinesin1 interacts with Arabidopsis atlastin RHD3 to move ER with plus-end of microtubules. *Nat. Commun.* **11**, 5510 (2020).
8. T. Wang *et al.*, Local zones of endoplasmic reticulum complexity confine cargo in neuronal dendrites. *Cell* **148**, 309–321 (2012).
9. M. A. Ashraf, M. Facette, Plant biology: BASL gives the plant nucleus a sense of direction. *Curr. Biol.* **30**, R1375–R1377 (2020).
10. E. R. Gomes, S. Jani, G. G. Gundersen, Nuclear movement regulated by Cdc42, MRCK, myosin, and actin flow establishes MTOC polarization in migrating cells. *Cell* **121**, 451–463 (2005).
11. K. Ishishita *et al.*, Phototropin2 contributes to the chloroplast avoidance response at the chloroplast-plasma membrane interface. *Plant Physiol.* **183**, 304–316 (2020).
12. C. B. Field, M. J. Behrenfeld, J. T. Randerson, P. Falkowski, Primary production of the biosphere: Integrating terrestrial and oceanic components. *Science* **281**, 237–240 (1998).
13. O. N. Borkhsenious, C. B. Mason, J. V. Moroney, The intracellular localization of ribulose-1, 5-bisphosphate carboxylase/oxygenase in *Chlamydomonas reinhardtii*. *Plant Physiol.* **116**, 1585–1591 (1998).
14. Y. Wang, D. J. Stessman, M. H. Spalding, The CO_2 concentrating mechanism and photosynthetic carbon assimilation in limiting CO_2: How Chlamydomonas works against the gradient. *Plant J. Cell Mol. Biol.* **82**, 429–448 (2015).
15. A. M. Geraghty, M. H. Spalding, Molecular and structural changes in Chlamydomonas under limiting CO_2 (a possible mitochondrial role in adaptation). *Plant Physiol.* **111**, 1339–1347 (1996).
16. D. Kramer, G. R. Findenegg, Variations in the ultrastructure of *Scenedesmus obliquus* during adaptation to low CO_2 level. *Z. Für Pflanzenphysiol.* **89**, 407–410 (1978).
17. I. Polukhina, R. Fristedt, E. Dinc, P. Cardol, R. Croce, Carbon supply and photoacclimation cross talk in the green alga *Chlamydomonas reinhardtii*. *Plant Physiol.* **172**, 1494–1505 (2016).
18. L. Wang, M. C. Jonikas, The pyrenoid. *Curr. Biol.* **30**, R456–R458 (2020).
19. P. Vance, M. H. Spalding, Growth, photosynthesis, and gene expression in Chlamydomonas over a range of CO_2 concentrations and CO_2/O_2 ratios: CO_2 regulates multiple acclimation states. *Can. J. Bot.* **83**, 796–809 (2005).
20. R. W. Kasili, A. K. Rai, J. V. Moroney, LCIB functions as a carbonic anhydrase: Evidence from yeast and Arabidopsis carbonic anhydrase knockout mutants. *Photosynth. Res.* **156**, 193–204 (2023), 10.1007/s11120-023-01005-1.
21. Y. Wang, M. H. Spalding, Acclimation to very low CO_2: Contribution of limiting CO_2 inducible proteins, LCIB and LCIA, to inorganic carbon uptake in *Chlamydomonas reinhardtii*. *Plant Physiol.* **166**, 2040–2050 (2014).
22. D. Duanmu, A. R. Miller, K. M. Horken, D. P. Weeks, M. H. Spalding, Knockdown of limiting-CO_2-induced gene HLA3 decreases HCO_3^- transport and photosynthetic Ci affinity in *Chlamydomonas reinhardtii*. *Proc. Natl. Acad. Sci. U.S.A.* **106**, 5990–5995 (2009).
23. B. Förster *et al.*, The *Chlamydomonas reinhardtii* chloroplast envelope protein LCIA transports bicarbonate in planta. *J. Exp. Bot.* **74**, 3651–3666 (2023), 10.1093/jxb/erad116.
24. A. Mukherjee *et al.*, Thylakoid localized bestrophin-like proteins are essential for the CO_2 concentrating mechanism of *Chlamydomonas reinhardtii*. *Proc. Natl. Acad. Sci. U.S.A.* **116**, 16915–16920 (2019).
25. M. A. Sinetova, E. V. Kupriyanova, A. G. Markelova, S. I. Allakhverdiev, N. A. Pronina, Identification and functional role of the carbonic anhydrase CAH3 in thylakoid membranes of pyrenoid of *Chlamydomonas reinhardtii*. *Biochim. Biophys. Acta* **1817**, 1248–1255 (2012).
26. T. Yamano, C. Toyokawa, D. Shimamura, T. Matsuoka, H. Fukuzawa, CO_2-dependent migration and relocation of LCIB, a pyrenoid-peripheral protein in *Chlamydomonas reinhardtii*. *Plant Physiol.* **188**, 1081–1094 (2022).
27. H. Fukuzawa *et al.*, CCM1, a regulatory gene controlling the induction of a carbon-concentrating mechanism in *Chlamydomonas reinhardtii* by sensing CO_2 availability. *Proc. Natl. Acad. Sci. U.S.A.* **98**, 5347–5352 (2001).
28. Y. Xiang, J. Zhang, D. P. Weeks, The *CIA5* gene controls formation of the carbon concentrating mechanism in *Chlamydomonas reinhardtii*. *Proc. Natl. Acad. Sci. U.S.A.* **98**, 5341–5346 (2001).
29. L. Wang *et al.*, Chloroplast-mediated regulation of CO_2-concentrating mechanism by Ca^{2+}-binding protein CAS in the green alga *Chlamydomonas reinhardtii*. *Proc. Natl. Acad. Sci. U.S.A.* **113**, 12586–12591 (2016).
30. W. Fang *et al.*, Transcriptome-wide changes in *Chlamydomonas reinhardtii* gene expression regulated by carbon dioxide and the CO_2-concentrating mechanism regulator CIA5/CCM1. *Plant Cell* **24**, 1876–1893 (2012).
31. K. Miura *et al.*, Expression profiling-based identification of CO_2-responsive genes regulated by CCM1 controlling a carbon-concentrating mechanism in *Chlamydomonas reinhardtii*. *Plant Physiol.* **135**, 1595–1607 (2004).
32. J. V. Moroney *et al.*, Isolation and characterization of a mutant of *Chlamydomonas reinhardtii* deficient in the CO_2 concentrating mechanism. *Plant Physiol.* **89**, 897–903 (1989).
33. M. Eisenhut, M.-S. Roell, A. P. M. Weber, Mechanistic understanding of photorespiration paves the way to a new green revolution. *New Phytol.* **223**, 1762–1769 (2019).
34. C. He *et al.*, Co-regulation of mitochondrial and chloroplast function: Molecular components and mechanisms. *Plant Commun.* **4**, 100496 (2023).
35. A. K. Rai, T. Chen, J. V. Moroney, Mitochondrial carbonic anhydrases are needed for optimal photosynthesis at low CO_2 levels in Chlamydomonas. *Plant Physiol.* **187**, 1387–1398 (2021).
36. S. V. Pollock, D. L. Prout, A. C. Godfrey, S. D. Lemaire, J. V. Moroney, The *Chlamydomonas reinhardtii* proteins CCP1 and CCP2 are required for long-term growth, but are not necessary for efficient photosynthesis, in a low-CO_2 environment. *Plant Mol. Biol.* **56**, 125–132 (2004).
37. A. Burlacot *et al.*, Alternative photosynthesis pathways drive the algal CO_2-concentrating mechanism. *Nature* **605**, 366–371 (2022).
38. A. Burlacot, G. Peltier, Energy crosstalk between photosynthesis and the algal CO_2-concentrating mechanisms. *Trends Plant Sci.* **28**, 795–807 (2023).
39. J. Harmon *et al.*, Intelligent image-activated sorting of *Chlamydomonas reinhardtii* by mitochondrial localization. *Cytometry A* **101**, 1027–1034 (2022), 10.1002/cyto.a.24661.
40. M. Á. Ruiz-Sola *et al.*, Light-independent regulation of algal photoprotection by CO_2 availability. *Nat. Commun.* **14**, 1977 (2023).
41. M. Shah, L. A. Chacko, J. P. Joseph, V. Ananthanarayanan, Mitochondrial dynamics, positioning and function mediated by cytoskeletal interactions. *Cell. Mol. Life Sci.* **78**, 3969–3986 (2021).
42. M. Onishi, J. R. Pringle, F. R. Cross, Evidence that an unconventional actin can provide essential F-actin function and that a surveillance system monitors F-actin integrity in Chlamydomonas. *Genetics* **202**, 977–996 (2016).
43. Y. Liu *et al.*, H+- and Na+- elicited rapid changes of the microtubule cytoskeleton in the biflagellated green alga Chlamydomonas. *Elife* **6**, e26002 (2017).
44. N. Birsa, R. Norkett, N. Higgs, G. Lopez-Domenech, J. T. Kittler, Mitochondrial trafficking in neurons and the role of the MIRO family of GTPase proteins. *Biochem. Soc. Trans.* **41**, 1525–1531 (2013).
45. J. D. Rochaix *et al.*, Nuclear and chloroplast mutations affect the synthesis or stability of the chloroplast psbC gene product in *Chlamydomonas reinhardtii*. *EMBO J.* **8**, 1013–1021 (1989).
46. N. D. Boisset *et al.*, Phosphoribulokinase abundance is not limiting the Calvin-Benson-Bassham cycle in *Chlamydomonas reinhardtii*. *Front. Plant Sci.* **14**, 1230723 (2023).
47. J. V. Moroney, B. J. Wilson, N. E. Tolbert, Glycolate metabolism and excretion by *Chlamydomonas reinhardtii*. *Plant Physiol.* **82**, 821–826 (1986).
48. T. Sun, H. Qiao, P.-Y. Pan, Y. Chen, Z.-H. Sheng, Motile axonal mitochondria contribute to the variability of presynaptic strength. *Cell Rep.* **4**, 413–419 (2013).
49. L. C. M. Mackinder *et al.*, A spatial interactome reveals the protein organization of the algal CO_2-concentrating mechanism. *Cell* **171**, 133–147.e14 (2017).
50. H. Treves *et al.*, A newly isolated Chlorella sp. from desert sand crusts exhibits a unique resistance to excess light intensity. *FEMS Microbiol. Ecol.* **86**, 373–380 (2013).
51. H. Nozaki, W. Mahakham, W. Heman, R. Matsuzaki, M. Kawachi, Morphology, mating system and taxonomy of Volvox africanus (Volvocaceae, Chlorophyceae) from Thailand. *Bot. Stud.* **63**, 1 (2022).
52. C. Uwizeye *et al.*, Morphological bases of phytoplankton energy management and physiological responses unveiled by 3D subcellular imaging. *Nat. Commun.* **12**, 1049 (2021).
53. G. Yu *et al.*, Mitochondrial phosphoenolpyruvate carboxylase contributes to carbon fixation in the diatom *Phaeodactylum tricornutum* at low inorganic carbon concentrations. *New Phytol.* **235**, 1379–1393 (2022).
54. M. Samukawa, C. Shen, B. M. Hopkinson, Y. Matsuda, Localization of putative carbonic anhydrases in the marine diatom, *Thalassiosira pseudonana*. *Photosynth. Res.* **121**, 235–249 (2014).
55. L. Wei *et al.*, RNAi-based targeted gene knockdown in the model oleaginous microalgae *Nannochloropsis oceanica*. *Plant J. Cell Mol. Biol.* **89**, 1236–1250 (2017).
56. L. Wei *et al.*, Transcriptomic and proteomic responses to very low CO_2 suggest multiple carbon concentrating mechanisms in *Nannochloropsis oceanica*. *Biotechnol. Biofuels* **12**, 168 (2019).
57. M. D. Burton, J. Moore, The mitochondrion of the flagellate, *Polytomella agilis*. *J. Ultrastruct. Res.* **48**, 414–419 (1974).
58. K. P. Gaffal, G. J. Schneider, Numerical, morphological and topographical heterogeneity of the chondriome during the vegetative life cycle of *Polytoma papillatum*. *J. Cell Sci.* **46**, 299–312 (1980).
59. N. J. Lang, Electron-microscopic demonstration of plastids in Polytoma. *J. Protozool.* **10**, 333–339 (1963).
60. T. Pánek *et al.*, A new lineage of non-photosynthetic green algae with extreme organellar genomes. *BMC Biol.* **20**, 66 (2022).
61. M. J. Devine, N. Birsa, J. T. Kittler, MIRO sculpts mitochondrial dynamics in neuronal health and disease. *Neurobiol. Dis.* **90**, 27–34 (2016).
62. R. L. Frederick, J. M. McCaffery, K. W. Cunningham, K. Okamoto, J. M. Shaw, Yeast Miro GTPase, Gem1p, regulates mitochondrial morphology via a novel pathway. *J. Cell Biol.* **167**, 87–98 (2004).
63. S. Yamaoka, C. J. Leaver, EMB2473/MIRO1, an Arabidopsis Miro GTPase, is required for embryogenesis and influences mitochondrial morphology in pollen. *Plant Cell* **20**, 589–601 (2008).
64. N. Nitta *et al.*, Intelligent image-activated cell sorting. *Cell* **175**, 266–276.e13 (2018).
65. X. Li *et al.*, A genome-wide algal mutant library and functional screen identifies genes required for eukaryotic photosynthesis. *Nat. Genet.* **51**, 627–635 (2019).

66. P. Crozet *et al.*, Birth of a photosynthetic chassis: A MoClo toolkit enabling synthetic biology in the microalga *Chlamydomonas reinhardtii*. *ACS Synth. Biol.* **7**, 2074–2086 (2018).
67. M. Schroda, D. Blöcker, C. F. Beck, The HSP70A promoter as a tool for the improved expression of transgenes in Chlamydomonas. *Plant J. Cell Mol. Biol.* **21**, 121–131 (2000).
68. N. Fischer, J. D. Rochaix, The flanking regions of psaD drive efficient gene expression in the nucleus of the green alga *Chlamydomonas reinhardtii*. *Mol. Genet. Genomics* **265**, 888–894 (2001).
69. E. Weber, C. Engler, R. Gruetzner, S. Werner, S. Marillonnet, A modular cloning system for standardized assembly of multigene constructs. *PLoS One* **6**, e16765 (2011).
70. D. N. Mastronarde, Automated electron microscope tomography using robust prediction of specimen movements. *J. Struct. Biol.* **152**, 36–51 (2005).
71. J. R. Kremer, D. N. Mastronarde, J. R. McIntosh, Computer visualization of three-dimensional image data using IMOD. *J. Struct. Biol.* **116**, 71–76 (1996).
72. G. Tang *et al.*, EMAN2: An extensible image processing suite for electron microscopy. *J. Struct. Biol.* **157**, 38–46 (2007).
73. T. D. Goddard *et al.*, UCSF ChimeraX: Meeting modern challenges in visualization and analysis. *Protein Sci. Publ. Protein Soc.* **27**, 14–25 (2018).